Accepted Manuscript

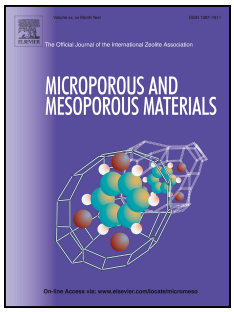

Catalytic activity of SnO_2- and SO_4/SnO_2-containing clinoptilolite in the esterification of levulinic acid

J. Pavlovic, M. Popova, R.M. Mihalyi, M. Mazaj, G. Mali, J. Kovač, H. Lazarova, N. Rajic

PII: S1387-1811(18)30634-6

DOI: https://doi.org/10.1016/j.micromeso.2018.12.009

Reference: MICMAT 9225

To appear in: *Microporous and Mesoporous Materials*

Received Date: 10 September 2018

Revised Date: 13 November 2018

Accepted Date: 7 December 2018

Please cite this article as: J. Pavlovic, M. Popova, R.M. Mihalyi, M. Mazaj, G. Mali, J. Kovač, H. Lazarova, N. Rajic, Catalytic activity of SnO_2- and SO_4/SnO_2-containing clinoptilolite in the esterification of levulinic acid, *Microporous and Mesoporous Materials* (2019), doi: https://doi.org/10.1016/j.micromeso.2018.12.009.

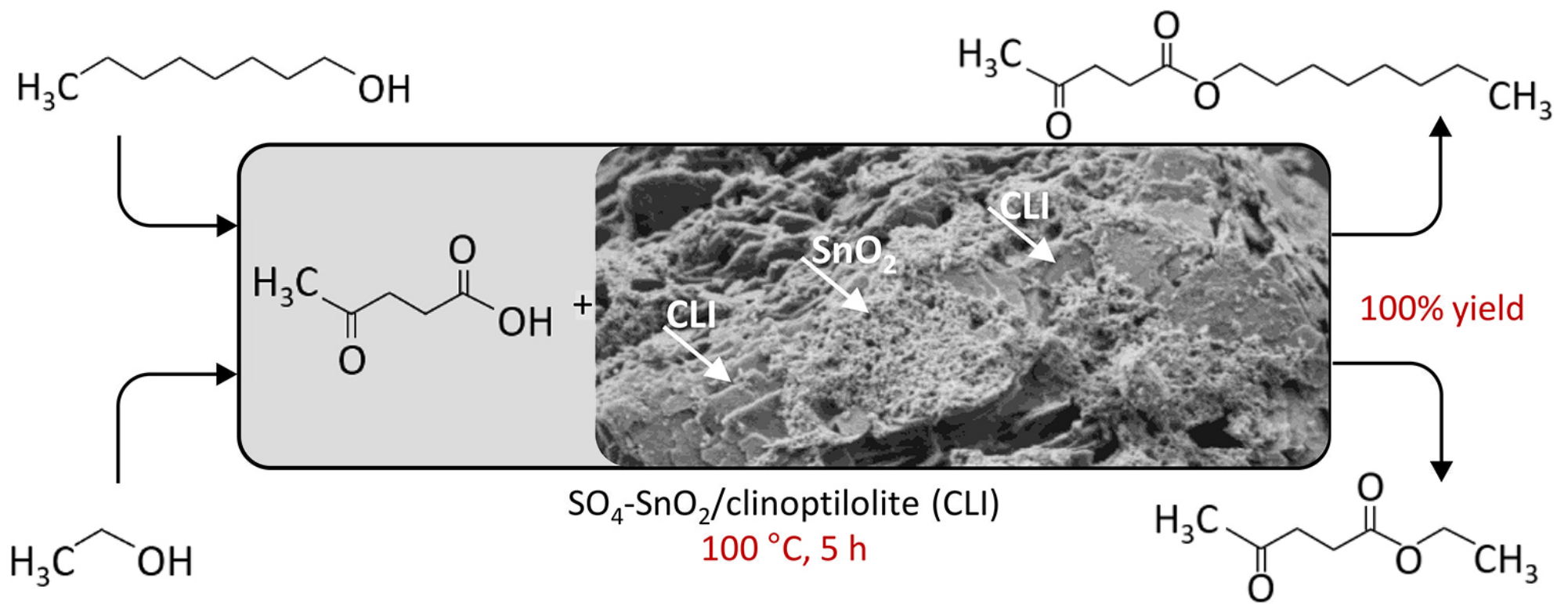
SnO2
CLI
CLI
100% yield
SO4-SnO2/clinoptilolite (CLI)
100 °C, 5 h

Catalytic activity of SnO_2- and SO_4/SnO_2-containing clinoptilolite in the esterification of levulinic acid

Pavlovic J.[a], Popova M.[b], Mihalyi R. M.[c], Mazaj M.[d], Mali G.[d], Kovač J.[e], Lazarova H.[b], and Rajic N.[f*]

[a]*Innovation Centre of the Faculty of Technology and Metallurgy, University of Belgrade, Karnegijeva 4, 11120 Belgrade, Serbia*

[b]*Institute of Organic Chemistry with Centre of Phytochemistry, Bulgarian Academy of Science, Acad. G. Bonchev, bl. 9, 1113 Sofia, Bulgaria*

[c]*Institute of Materials and Environmental Chemistry, Research Centre for Natural Sciences, Hungarian Academy of Sciences, Magyar Tudosok korutja 2, Budapest 1117, Hungary*

[d]*National Institute of Chemistry, Hajdrihova 19, 1000 Ljubljana, Slovenia*

[e]*Jozef Stefan Institute, Jamova 39, Ljubljana, Slovenia*

[f]*Faculty of Technology and Metallurgy, University of Belgrade, Karnegijeva 4, 11120 Belgrade, Serbia*

Corresponding author*: E-mail address: nena@tmf.bg.ac.rs. Full postal address: Faculty of Technology and Metallurgy, University of Belgrade, Karnegijeva 4, 11120 Belgrade, Serbia.

ABSTRACT

Catalysts based on natural zeolite – clinoptilolite loaded with either SnO_2 (TOHCLI) or sulfated SnO_2 (STOHCLI) were prepared and tested in the esterification of levulinic acid (LA) with octanol or ethanol. The Sn content in TOHCLI and STOHCLI varied from 4.5 to 12.3 wt.%. The catalysts were characterized by powder X-ray diffraction method, scanning electron microscopy coupled with energy dispersive X-ray spectroscopy, thermal analysis, X-ray photoelectron spectroscopy, N_2 physisorption at –196 ^{o}C, ^{27}Al and ^{29}Si MAS NMR solid state spectroscopy and FTIR spectroscopy for analysis of acidic centers. A high conversion rate of LA into octyl- (OLA) or ethyl levulinate (ELA) was obtained for both TOHCLI and STOHCLI. TOHCLI showed a high activity in the conversion of LA into OLA (55 %) and a moderate activity in the conversion to ELA (22 %). STOHCLI led to a total conversion of LA to OLA and ELA due to the presence of a high amount of Brønsted and Lewis acid sites in the catalysts. The catalytic activity decreased to 86 % for OLA and to 66 % for ELA after next five cycles. Lower catalytic activity in the repeated cycles during ELA formation was explained by pore blockage due to coke formation.

Keywords: renewable levulinic acid, sulfated SnO_2, clinoptilolite, esterification, biolubricant production

1. Introduction

Levulinic acid (LA) is very important platform chemicals due to ease of preparation from biomass and its reactivity. LA has a great potential for production of valuable chemicals for the food and chemical industries [1, 2]. Alkyl levulinates are of particular interest due to their specific physicochemical properties which make them applicable as fuel additives, solvents, and plasticizers [3, 4].

Levulinate esters can be obtained by esterification of LA with primary alcohols such as ethanol, butanol or octanol at room temperature. However, very slow kinetics of the esterification requires using of an acid catalyst. Conventionally, strong mineral acids (usually H_2SO_4) have been used for the purpose [5]. However, drawbacks associated with environmental problems necessitate a replacement of the acids by more suitable catalysts, which would be less corrosive and reusable such as heterogeneous ones. Accordingly, investigations of suitable heterogeneous catalysts for the esterification of levulinic acid have attracted a great attention.

Due to their thermal stability, shape-selectivity and adaptive acidity zeolites are good candidates for catalysts for esterification of LA. Fernandes et al. [6] studied zeolites with different pore structure (HUSY, HBEA, HMOR, HZSM-5, HMCM-22), different sulfated oxides with super acidity (SO_4-ZrO_2, SO_4-Nb_2O_5, SO_4-TiO_2, SO_4-SnO_2) and Amberlyst-15 in the conversion of LA to ELA. A correlation between acidity and catalytic activity was found for the super acid oxides whereas for the studied zeolites only geometry of the pore systems had a significant role. Among the tested catalysts, a remarkable yield of ELA was obtained with the Amberlyst-15 and sulfated SnO_2 which was ascribed to the acidity of sulfate groups. Very recently, Popova et al. [7] has also found that sulfated SnO_2 is catalytically active in the conversion of LA to

ELA. The activity was attributed to the synergistic action of Lewis and Brønsted acid sites. Moreover, sulfated zirconia supported on mesoporous KIL-2 was found to be active in the conversion of LA into ELA and BLA [8]. The activity was ascribed to the presence of strong Brønsted acid centers. Patil et al. [9] demonstrated the significance of geometry of the pore system. In a series of bimodal micro-mesoporous HBEA a crucial role of the mesopore system was reported in the conversion of LA into ELA. Importance of the pore size in the conversion of LA to BLA was also reported for HBEA, HY, HZSM-5, HMOR [10, 11].

Heteropolyacids such as dodecatungestophosphoric acid supported or incorporated into different matrices [12, 13], commercial acidic sulfonic poly(styrene-co-divinylbenzene) resins (PS-DVB) [14], sulfonic mesoporous silicas [15], Al-MCM-41 were also tested in the esterification of LA to ELA [16]. Selected literature data obtained under experimental conditions similar to that used in this study are summarized in Table 1.

Table 1

Until now most studies regarding catalytic conversion of LA to levulinate esters have been focused to ELA and BLA [6, 8, 17]. Data for the conversion of LA to OLA have been rather scarce [18, 19] although OLA has been recognized as an important biolubricant. Its specific properties such as a high flash point, high lubricity, very low volatility, high viscosity index and its biodegradability recommend OLA as a suitable replacement for synthetic and mineral-oil based lubricants.

To the best of our knowledge, natural zeolite – clinoptilolite has not been studied in the preparation of catalysts for the esterification of LA. The aim of the present study was to prepare a catalyst based on the low cost clinoptilolite and SnO_2 or on the sulfated SnO_2-containing clinoptilolite and to test them in the esterification of LA with octyl (Oct) and ethyl (Et) alcohol.

2. **Experimental**

2.1 Materials

Zeolitic tuff (CLI) from Serbia (Slanci deposit, Belgrade) was used as the clinoptilolite source. Semi-quantitative X-ray powder diffraction analysis (using the Rietveld refinement and the Topas□Academic v.4 software [20] gave for CLI (wt. %): clinoptilolite - 80, feldspars -16 and quartz - 4. The cation exchange capacity (CEC) measured by a standard procedure using the ion exchange with ammonium acetate was determined to be 160 meq/100 g.

Prior to the experiments, CLI was sieved and washed with deionized water, and dried overnight at 105 °C until a constant mass. Particle size in the range of 0.063-0.125 mm was chosen for the experiments. All used chemicals were of analytical grade.

2.2 Preparation of catalysts

A procedure includes the following steps: a) conversion of CLI to an acid form (HCLI); b) preparation of the SnO_2-containing CLI (TOHCLI); c) sulfation of TOHCLI (STOHCLI).

a. Conversion of CLI to HCLI

A triple treatment of CLI with 1 mol dm^{-3} HCl at 100 °C for 4 h using a solid/liquid mass ratio of 1:70 was followed by a treatment with 0.2 mol dm^{-3} NH_4OH at 65 °C for 0.5 h (solid/liquid ratio=1:30). The obtained HCLI was separated and dried at 80 °C until a constant mass.

b. Preparation of SnO_2-containing CLI (TOHCLI)

Samples of TOHCLI with approx. 5–12 wt.% of Sn were prepared following a slightly modified method described by Matatsushashi [21] and Sowmiya [22]. HCLI was suspended in deionized water using a solid/liquid mass ratio 1:100 and stirred for about 10 min. The pH of the suspension was adjusted to 10 by dropwise addition of a 25 wt. % NH_4OH. Then, an ethanolic solution of $SnCl_2 \cdot 2H_2O$ (C_0=2 g dm^{-3}) was added dropwise under stirring. The pH was kept constant. The added volumes of C_0 were varied from 100 to 250 cm^3 in order to obtain TOHCLI with different amounts of Sn. The suspensions were separated by centrifugation after 24 h of stirring, washed with 4 wt.% CH_3COONH_4 and then with deionized water until chloride free. TOHCLI samples were dried overnight at 120 °C and then calcined at 400 °C for 2 h. The samples were denoted as TOHCLI5, TOHCLI9 and TOHCLI12 where numbers refer to different Sn contents: TOHCLI5 - 4.5 wt.%, TOHCLI9 - 9.2 and TOHCLI12 - 12.3.

c. Preparation of sulfated TOHCLI (STOHCLI)

TOHCLI5, TOHCLI9 or TOHCLI12 were suspended in 3 mol dm^{-3} $(NH_4)_2SO_4$ to obtain a solid/liquid mass ratio of 1:50 and stirred at room temperature for 24 h. Then, the solids were separated by centrifugation, washed, dried overnight at 120 °C to a

constant mass, and calcined for 2 h at 400 °C. The obtained products were denoted as STOHCLI5, STOHCLI9 and STOHCLI12 where the numbers refer the content of Sn.

2.3 Characterization

X-ray diffraction analysis

Powder X-ray diffraction (PXRD) patterns of the samples were recorded using an APD2000 Ital Structure diffractometer with CuKα radiation (λ = 0.15418 nm). Scans were performed in the 2θ range 5–50° with a step of 0.02 ° per 1 s.

Energy dispersive X-ray spectroscopy (EDS)

Elemental analyses were performed using a Carl Zeiss Supra™ 3VP field-emission gun scanning electron microscope (FEG-SEM) equipped with EDS detector (Oxford Analysis) with INCA Energy system for quantification of elements.

Thermal analysis

A simultaneous thermogravimetry (TGA) and differential thermal analysis (DTA) was performed in order to obtain a deeper insight into thermal events during conversion of the Sn-loaded HCLI to TOHCLI. The analysis was performed using a SDT Q-600 instrument (TA Instruments). The samples were heated in opened alumina cups (90 µl) from the room temperature to 700 °C at a heating rate of 10 °C min^{-1} under synthetic air (100 ml min^{-1}).

X-ray photoelectron spectroscopy

The X-ray photoelectron spectroscopy (XPS) analyses were carried out on a PHI–TFA XPS spectrometer produced by Physical Electronics Inc. Powders were on carbon adhesion tape used for SEM microscopy and introduced in ultra-HV spectrometer. The vacuum during the XPS analyses was in the range of 10–9 mbar. The analyzed area was 0.4 mm in diameter and the analyzed depth was about 3–5 nm. Sample surfaces were excited by X-ray radiation from monochromatic Al source at photon energy of 1486.6 eV. The survey wide-energy spectra were taken over an energy range of 0–1200 eV with pass energy of analyzer of 187 eV in order to identify and quantify present elements on the surface. The high-energy resolution spectra were acquired with energy analyzer operating at resolution of about 0.6 eV and pass energy of 29 eV. During data processing the spectra were aligned by setting the C 1s peak at 284.8 eV, characteristic for C-C/C-H bonds. The accuracy of binding energies was about ±0.3 eV. Quantification of the surface composition was performed from XPS peak intensities taking into account the relative sensitivity factors provided by instrument manufacturer [23]. XPS spectra were analyzed by a MultiPak software. High resolution spectra were fitted with Gauss-Lorentz functions and Shirley function was used for background removal. In order to analyse the in-depth distribution of elements in the sub-surface region up to 25 nm deep, the XPS depth profiling was performed in combination with ion sputtering. The Ar ions of energy 4 keV were used. The velocity of the ion sputtering was estimated to be 1.0 nm min^{-1} calibrated on the Ni/Cr multilayer structure of the known thickness.

Solid-state NMR spectroscopy

Solid-state NMR experiments were carried out on a 600 MHz Varian NMR system equipped with a 3.2 mm Varian HX CPMAS probe. Larmor frequencies for ^{27}Al and ^{29}Si nuclei were 156.20 MHz and 119.09 MHz, respectively. For ^{27}Al magic-angle spinning (MAS) measurements excitation pulse of 0.8 µs was used, number of scans was 3000 and repetition delay between scans was 1 s. Sample rotation frequency was 16 kHz. For ^{29}Si MAS measurements excitation pulse was 2.8 µs, repetition delay was 60 s, and number of repetitions was 2400.

Textural properties

Porosity characteristics were determined by N_2 adsorption at –196 °C using a Micromeritics Instrument (ASAP 2020). Prior to the measurements, the samples were degassed for 4 h at 200 °C under high vacuum. The specific surface area of sample (S_{BET}) was calculated according to the Brunauer, Emmett, Teller (BET) method up to relative pressures $p/p_0 = 0.15$. The total pore volume (V_{tot}) was given at $p/p_0 = 0.99$. Pore size distribution was analyzed according to the Barrett, Joyner and Halenda method (BJH) from the adsorption isotherms.

Acidity measurements

Surface acidity was examined by FTIR using a Nicolet Impact Type 400 spectrometer, applying a self-supported wafer technique using pyridine (Py) as the probe molecule. Concentration of surface acid sites was determined from FTIR spectra.

FTIR spectra were recorded at room temperature averaging 32 scans at a resolution of 2 cm^{-1}. Spectra were normalized to a wafer thickness of 5 mg cm^{-2}. Before the Py

adsorption the samples were evacuated in a high vacuum (HV, < 10^{-6} mbar) for 1 h at 400°C, then treated with Py at 50 mbar and degassed in HV for 0.5 h at 100 °C, 200 °C, 300 °C and 400 °C. After evacuation spectra were recorded at room temperature.

2.4 Catalytic experiments

Conversion of LA into OLA and ELA was carried out in a batch reactor with magnetic stirrer under reflux. Prior to the catalytic test, the catalysts were pre-treated *ex-situ* in oven for at 1 h at 200 °C, at static conditions. The reaction was performed under conditions which were similar to those previously found to be the optimal ones [8]. In a typical experiment, the reactor was charged with 1 g. LA, 7 ml ethanol or octanol and 0.2 g powder catalyst while the LA/ethanol (octanol) weight ratio was maintained 1:7. The reactor was placed in an oil bath, heated under stirring with 200 rpm at the reaction temperature of 100 °C for 5 h. The thermocouple was positioned in the reaction mixture for accurate measurement of the reaction temperature. Samples were taken at chosen time intervals and analyzed using HP-GC with a flame ionization detector equipped with a WCOT FUSED SILICA 25m x 0.25mm COATING CP-SIL 43CB column. Analyses were carried out using nitrogen as a carrier gas and manual injection (the sample volume injected was 1 μl). The following temperature profile was used: column temperature set from 100 to 200 °C (20 °C min^{-1}), the injector and detector temperature was 250 and 300 °C, respectively. The LA conversion rate was determined using the LA/OLA or LA/ELA area ratio. At the end of the reaction, the reactor was cooled to room temperature and the catalyst was recovered by centrifugation. The mass balance was made on the basis of carbon-containing products.

2.5 Catalyst reusability

Reusability was tested for STOHCLI9 in six reaction cycles (one with the fresh catalyst and five repeated cycles with the reused catalyst). After completion of the reaction in each cycle, the catalyst was separated by centrifugation, washed with acetone, dried at 60 ºC for 5 h and calcined at 400 °C in air for 3 h.

3. **Results and discussion**

3.1 Characterization of the catalysts

PXRD patterns (given in Supplementary materials) show that crystallinity of the clinoptilolite remains intact after the conversion of CLI to HCLI. Further modification of HCLI into TOHCLI causes a slight loss of the crystallinity which remains unaffected by conversion of TOHCLI into STOHCLI.

Average chemical compositions of the clinoptilolite phase of all the studied samples obtained by EDS are shown in Table 2. Conversion of CLI to HCLI causes a partial dealumination of the clinoptilolite lattice which is evident by the Si/Al molar ratio which is higher in the modified samples than in the parent CLI. Also, the content of Na decreased significantly and K, Ca and Mg were not detected after the conversion to HCLI. These confirm the fact that CLI is mostly converted into HCLI. Sulfation of TOHCLI causes a partial leaching of Sn. The leaching extent varies from 43% (STOHCLI5), 13% (STOHCLI9) and 25% (STOHCLI12). The molar ratio of S/Sn (Table 2) indicates that a partial sulfation of TOHCLI was achieved and the S/Sn molar ratio decreases with the increase of Sn content. A similar phenomenon was reported for the sulfated ZrO_2-containing KIL–2 [8]. The lowest S/Zr molar ratio (0.4) was found for the highest amount of the loaded Zr. Lower sulfation extent in the STOHCLI samples

with a higher Sn content could be ascribed to a poor accessibility of Sn within the clinoptilolite structure.

Table 2

Conversion of the Sn-loaded HCLI to TOHCLI was studied by thermal analysis (Fig. 1a and b). It is evident that the total weight loss increases with the Sn increase from 10.9 (TOHCLI5) to 12.2 wt.% (TOHCLI12). DTG curves display three maxima at about 60, 320 and 500 ºC which can be assigned to the following events: 1) loss of physically adsorbed water (6.5 wt.%) at temperatures below 100 ^{o}C, 2) dehydroxylation which occurs in the temperature range 200–400 °C, and 3) formation of the Sn oxide species at 500 °C. The last event is assumed on the basis of our previous studies where we found that the DTG maximum at about 500 °C reflects crystallization of different oxide species in the clinoptilolite matrix [24]. Formation of the Sn oxide species was confirmed by further analyses (*vide infra*).

DTG and TG curves of the TOHCLI samples after sulfation (Fig. 1c and d) display two resolved DTG maxima in temperature range 200–400 °C which can be due to the presence of coordinated water molecules strongly bound to sulfate groups. The maximum in the 400-600 ^{o}C temperature range can be ascribed to the decomposition of sulfate to SOx species [25, 26]. The corresponding weight loss increased with the increase of the Sn content and was 2.9 wt.% for STOHCLI5 and 3.5 wt.% for STOHCLI12.

Fig. 1

XPS analyses confirm the presence of SnO_2 in the STOHCLI samples. The analysis for STOHCLI5 and STOHCLI9 is presented in Fig. 2. The Sn 3d spectra (Fig. 2) reveal two peaks located at 487.4 and 495.8 eV for STOHCLI5, and 487.5 and 496.0 eV for STOHCLI9 which can be assigned to Sn $3d_{5/2}$ and Sn $3d_{3/2}$, respectively. The spectra are in accordance with the literature [27, 28], confirming the presence of the SnO_2 species in dealuminated zeolites. The XPS depth profiles for STOHCLI5 show a small accumulation of Sn at the surface and a decrease of the Sn concentration from top to bottom. More pronounced Sn surface accumulation is evident in the sample with a higher Sn content (STOHCLI9). The presence of Sn inside the samples was unexpected and it indicates that the Sn species are not present only at the surface of the zeolite but also inside the lattice. A similar phenomenon was reported for the Sn(IV)-modified zeolite Beta [29, 30]. A two-step modification which included dealumination and impregnation of the zeolite with $SnCl_4$ created holes in the zeolite lattice. It was assumed that inside these holes the Sn(IV) species form covalent Si–O–Sn bonds with the zeolite lattice.

Fig. 2

According to the NMR results (*vide infra*) a similar phenomenon could be suggested during the formation of TOHCLI.

Fig. 3

^{27}Al MAS NMR spectra of the representative samples (HCLI, TOHCLI9 and STOHCLI9) are shown in Fig. 3a. As can be seen, three broad peaks at around 55, 30

and 0 ppm are evident in all the spectra. The peak at 55 ppm is characteristic for Al atoms located in tetrahedral positions of the zeolite framework (AlO_4 structural units). The peak at 0 ppm corresponds to octahedrally coordinated extra-framework Al species (AlO_6 structural units), which were formed by dealumination of the clinoptilolite framework during conversion of CLI into HCLI [31–33]. Also, the peak at around 30 ppm can be ascribed to the extra-framework five-coordinated Al. In the spectrum of TOHCLI9 an additional peak appears. It can be related to the hexa-coordinated aluminum species surrounded by SiO species [31, 34]. All this suggests that such extra-framework Al–O–Si species exist in the TOHCLI9 and contribute to Lewis acidity. The ^{29}Si MAS NMR spectra are almost identical for all analyzed samples (Fig. 3b) exhibiting peaks associated with different Si environments. ^{29}Si NMR spectra fitted with three contributions show resonances at about -110, -101 and -92 ppm. The peaks at -101 ppm and -92 ppm can be assigned to the Si atoms that have H atoms in their vicinity (Q^3 and Q^2 sites, $(OSi)_3Si(OH)$ and $(OSi)_2Si(OH)_2$, respectively), whereas the peak at -110 ppm belongs to Q^4 and represents the species $Si(OSi)_4$.

Textural properties were studied by the N_2 adsorption/desorption isotherms. Representative results are given in Fig. 4, and textural parameters determined from the isotherms are given in Table 3. Based on the IUPAC classification, all samples exhibit adsorption isotherms of the type IV [35] that are typical for zeolitic materials containing both micropores due to structural features of the framework, and mesopores introduced by different modification processes including dealumination. As can be seen from Table 3, an increase of the specific surface area with the increase of the Sn amount in TOHCLI samples is evident especially for the highest Sn amount. This can be explained by an influence of the modification procedure which caused agglomeration of the

zeolite particles, thereby significantly increasing the S_{ext} value, predominantly for TOHCLI12. Moreover, a small decrease in the specific surface area of the STOHCLI samples in comparison to TOHCLI is evident. This can be assigned to a partial pore blockage caused by sulfate groups. The decrease of the specific surface area varies from 3% for STOHCLI5 to about 20% for STOHCLI9.

Fig. 4

Table 3

The nature of the acidic species in the catalysts was determined by FTIR spectra of adsorbed Py. The spectra of nonsulfated (TOHCLI5 and TOHCLI9) and sulfated catalyst (STOHCLI5 and STOHCLI9) are given in Fig. 5. The Lewis acid sites can be associated with the ring vibrations of coordinatively bound Py at 1615 and 1452 cm^{-1} (LPy), while Brønsted acid sites (BPy) exhibit bands at 1638 and 1550 cm^{-1} [36]. The spectra of nonsulfated samples contain bands characteristic for both Lewis and Brønsted acid sites. The amount of Lewis acid sites of nonsulfated catalysts is much higher than Brønsted acid sites (Table 4), originating from coordinatively unsaturated Sn ions on the clinoptilolite [8, 37]. Higher amount of Sn in HCLI led to an increase of the amount of Lewis acid sites, whereas Brønsted acid sites did not increase significantly.

Both Lewis and Brønsted acid sites are present in the sulfated samples. In comparison to nonsulfated samples, the amounts of Lewis and Brønsted acid sites are significantly higher for sulfated samples, suggesting that sulfate species act as Lewis acid sites and also increase Brønsted acid strength of the hydroxyl groups on the surface

of tin oxide particles. Similar effect was observed for sulfated ZrO_2/KIL-2 and sulfated nano-SnO_2 [7,8].

Fig. 5

Table 4

3.2 Catalytic activity

Fig. 6 shows the esterification of LA into OLA in the presence of TOHCLI and STOHCLI. The studied samples are catalytically active in the esterification reaction in contrast to non-modified HCLI which showed very low catalytic activity (less than 10 %) after 5 h with both Oct and Et (not shown).

For all the TOHCLI samples the conversion after 5 h is about 55% indicating that in the studied range Sn concentration does not affect the catalytic activity. This can be explained by the fact that modification by more than 4.5 wt.% Sn leads to the Sn deposition inside the pores or on the zeolite walls where the Sn species are not accessible for the reactant molecules. According to the XPS data deposition of the Sn species occurs not only at the surface but also inside the clinoptilolite lattice. Relatively high catalytic activity of the TOHCLI could be ascribed to the presence of relatively high amounts of Lewis acid sites. However, although the amounts of Lewis acid sites increased by increasing the Sn content (Table 4) the conversion rate did not increase indicating that all acid sites are not available for the esterification.

Total conversion of LA into OLA in the presence of both STOHCLI samples indicates similar acidity of the samples which is in accord with the FTIR spectroscopic

measurements. Similar amounts of Brønsted and Lewis acid sites are evident for STOHCLI5 and STOHCLI9.

Moreover, significant higher amounts of both acid sites for STOHCLI in comparison to TOHCLI can be responsible for higher conversion obtained for STOHCLI (100%) than for TOHCLI (55%). As a comparison, the sulfated ZrO_2/KIL–2 showed a significantly higher conversion of LA into ELA and BLA compared to the non-sulfated samples which was attributed to higher acidity of the sulfated catalyst [8].

Fig. 6

Fig. 7 shows the esterification of LA into ELA in the presence of TOHCLI and STOHCLI. Activity of TOHCLI in the conversion LA to ELA is significantly lower than in the conversion to OLA. Also evident is the influence of the Sn content on the catalytic activity as the conversion increases by increasing of the Sn content. This could be ascribed to the fact that catalytic active acid sites become more accessible to smaller ethanol molecules. The conversion to ELA is significantly higher for STOHCLI samples which is due to the presence of both Brønsted and Lewis acid sites. These results confirm suggestion that the presence of sulfate groups significantly influences the conversion of LA into ELA [7,8].

Fig. 7

3.2 Reusability of the catalysts

Reuse of the catalysts was tested for STOHCLI9. In the esterification with Oct, the catalytic activity decreased from 100% (fresh catalyst) to 86% after next five cycles. The decrease can be assigned to a partial leaching of sulfate groups as reflected in the decrease of the S/Sn molar ratio (from 0.4 to 0.2) (Table 2). There was no further sulfate leaching after the second cycle, suggesting that further desulfation is most probably prevented by structural features of the partially dealuminated clinoptilolite lattice. Crystallinity of the spent STOHCLI9 was checked by XRD confirming that the catalyst remained crystallographically unchanged (diffractogram is given in Supplementary materials).

The conversion of LA to ELA on STOHCLI9 decreases from 94% (fresh catalyst) to 68% after the first cycle and is stabilized at 66% in the next five cycles (Fig. 8). The catalytic activity in the LA conversion to ELA is lower than to OLA and the conversion rate decreases after the second cycle to 66 %. It seems likely that the esterification with Et occurs not only on the external surface of the catalyst but also in the pores because of the appropriate sizes of the LA and Et molecules which can penetrate in the pores. However, the formation of intermediate products and ELA is blocked in the pores and their diffusion out is hindered which most probably results in coke formation and decreasing of catalytic activity. Thus, the coke formation most probably decreases catalytic activity.

Esterification of LA with Oct proceeds in a different manner. The longer chain of the Oct molecules cannot penetrate the pores and the process occurs only on the external surface of the catalyst. In this case the process is faster and the coke formation is significantly lower. According to thermal analysis (not shown) of the spent catalysts the

residue after the OLA production is significantly lower (14 wt.%) than after ELA (26 wt.%).

Fig. 8

The obtained results show that natural zeolite - clinoptilolite as cheap and available material can be used in the preparation of catalysts for the LA esterification. Clinoptilolite matrix prevents the agglomeration of sulfated SnO_2 species offering a higher dispersion which provides better accessibility for the reactants. Furthermore, in contrast to moderate catalytically sulfated oxides which reusability is limited [6, 8], SnO_2 and sulfated SnO_2 supported on the clinoptilolite can be used as effective and reusable catalysts for the esterification of LA with ethanol and octanol.

4. **Conclusions**

The catalysts based on the low cost natural zeolite - clinoptilolite and SnO_2 or sulfated SnO_2 showed high catalytic activities in the esterification of LA into levulinates. Catalytic activity of non sulfated samples in the OLA production was not significantly affected by the Sn content, exhibiting catalytic activity around 55 %. The lack of influence of the Sn content was ascribed to the hindered access of long chain of Oct molecules to the acid sites in the pores of catalysts. A total conversion of LA to OLA was obtained for all sulfated SnO_2-containing clinoptilolite samples due to the presence of a high amount of Brønsted and Lewis acid sites. The stable catalytic activity found in five repeated reaction cycles suggests that the initial leaching of sulfate groups from the catalyst was preserved due structural features of the clinoptilolite lattice. The

prepared catalysts show higher catalytic activity in the esterification of LA to OLA than to ELA which is due to a higher coke formation in the latter process.

Acknowledgments

This work was supported by the Ministry of Education, Science and Technological Development of the Republic of Serbia (Project No. 172018), the Slovenian Research Agency (research core funding No. P-0021) and COST Action FP1306 ”Valorisation of lignocellulosic biomass side streams for sustainable production of chemicals, materials & fuels using low environmental impact technologies”.

References

[1] D.W. Rackemann, W.O.S. Doherty, Biofuel. Bioprod. Bior. 5 (2011) 198–214.

[2] K. Yan, C. Jarvis, J. Gu, Y. Yan, Renew. Sust. Energ. Rev. 51 (2015) 986–997.

[3] J.J. Bozell, L. Moens, D.C. Elliopt, Y. Wang, G.G. Neuenscwander, S.W. Fitzpatric, R.J. Bilski, J.L. Jarnefels, Resour. Conserv. Recy. 28 (2000) 227–239.

[4] A. Démolis, N. Essayem, F. Rataboul, ACS Sustain. Chem. Eng. 2 (2014) 1338–1352.

[5] H.J. Bart, J. Reidetschlagerj, K. Schatkaj, A. Lehmannt, Ind. Eng. Chem. Res. 3 (1994) 21–25.

[6] D.R. Fernandes, A.S. Rocha, E.F. Mai, C.J.A. Mota, V. Teixeira da Silva, Appl. Catal. A-Gen. 425–426 (2012) 199–204.

[7] M. Popova, P. Shestakova, H. Lazarova, M. Dimitrov, D. Kovacheva, A. Szegedi, G. Mali, V. Dasireddy, B. Likozar, N. Wilde, R. Gläser, Appl. Catal. A-Gen, 560 (2018) 119–131.

[8] M. Popova, A. Szegedi, H. Lazarova, A. Ristić, Y. Kalvachev, G. Atanasova, N. Wilde, N. Novak Tušar, R. Gläser, Micropor. Mesopor. Mat. 235 (2016) 50–58.

[9] C.R. Patil, P.S., Niphadkar, V.V. Bokade, P.N. Joshi, Catal. Commun. 43 (2014) 188–191.

[10] K.C. Maheria, J. Kozinski, A. Dalai, Catal. Lett. 143 (2013) 1220–1225.

[11] K.Y. Nandiwale, V.V. Bokade, Chem. Eng. Technol. 38 (2015) 246–252.

[12] S. Dharne, V.V. Bokade, J. Nat. Gas Chem. 20 (2011) 18–24.

[13] G. Pasquale, P. Vázquez, G. Romanelli, G. Baronetti, Catal. Commun. 18 (2012) 115–120.

[14] M.A. Tejero, E. Ramírez, C. Fité, J. Tejero, F. Cunill, Appl. Catal. A-Gen. 517 (2016) 56–65.

[15] J.A. Melero, G. Morales, J. Iglesias, M. Paniagua, B. Hernández, S. Penedo, Appl. Catal. A-Gen. 466 (2013) 116–122.

[16] A. Najafi Chermahini, M. Nazeri, Fuel Process. Technol. 167 (2017) 442–450.

[17] Y. Kuwahara, T. Fujitani, H. Yamashita, Catal. Today 237 (2014) 18–28.

[18] K.Y. Nandiwale, S.K. Yadava, V.V. Bokade, J. Energy Chem. 23 (2014) 535–541.

[19] L. Zhou, Y. He, L. Ma, Y. Jiang, Z. Huang, L. Yin, J. Gao, Bioresource Technol. 247 (2018) 568–575.

[20] A. Coelho, TOPAS Academic 4.1, Coelho Software, Brisbane, Australia, 2007.

[21] H. Matsuhashi, H. Miyazaki, Y. Kawamur, H. Nakamura, K. Arata, Chem. Mater. 13 (2001) 3038–3042.

[22] M. Sowmiya, A. Sharma, S. Parsodkar, B.G. Mishra, A. Dubey, Appl. Catal. A-Gen. 333 (2007) 272–280.

[23] J.F. Moulder, W.F. Stickle, P.E. Sobol, K. D. Bomben, Handbook of X-Ray Photoelectron Spectroscopy, Physical Electronics Inc. Eden Prairie, third ed., Minnesota, USA, 1995.

[24] N. Rajić, N. Zabukovec Logar, A. Rečnik, M. El-Roz, F. Thibault-Starzyk, P. Sprenger, L. Hannevold, A. Andersen, M. Stocker, Micropor. Mesopor. Mat. 176 (2013) 162–167.

[25] R. Gutiérez-Báez, J.A. Toledo-Antonio, M.A. Cortes-Jácome, P.J. Sebastian, A. Vázquez Langmuir, 20 (2004) 4265–4271.

[26] W. Shi, J. Li, Catal. Lett. 143 (2013) 1285–1293.

[27] B. Mallesham, P. Sudarsanam, G. Raju, B.M. Reddy, Green Chem. 15 (2013) 478–489.

[28] R. Rajalakshmi, V. Vasudevan Srinivasan, M.P. Pachamuthu, R. Maheswari, Mater. Chem. Phys. 154 (2015) 164–169.

[29] J. Dijkmans, J. Demol, K. Houthoofd, S. Huang, Y. Pontikes, B. Sels, J. Catal. 330 (2015) 545–557.

[30] F.F. Guan, T.T. Ma, X. Yuan, H.Y. Zeng, J. Wu, Catal. Lett. 148 (2018) 443–453.

[31] E. Lippmaa, A. Samoson, M. Magi, J. Am. Chem. Soc. 108 (1986) 1730–1735.

[32] T. Farías, A.R. Ruiz-Salvador, L. Velazco, L.C. de Ménorval, A. Rivera, Mater. Chem. Phys. 118 (2009) 322–328.

[33] Y. Garcia-Basabe, I. Rodriguez-Iznaga, L.C. de Menorval, Ph. Llewellyn, G. Maurin, D.W. Lewis, R. Binions, M. Autie, A.R. Ruiz-Salvador, Micropor. Mesopor. Mat. 135 (2010) 187–196.

[34] D. Zhang, A. Duan, Z. Zhao, C. Xu, J. Catal. 274 (2010) 273–286.

[35] K.S.W. Sing, D.H. Everett, R.A.W. Haul, L. Moscou, R.A. Pierotti, J. Rouquerol, T. Siemieniewska, Pure Appl. Chem. 57 (1985) 603–619.

[36] H.G. Karge, E. Geidel, in: H.G. Karge, J. Weitkamp (Eds.), Molecular Sieves 4, Characterization I, Springer, Berlin, 2003, pp. 1–201.

[37] E.E. Platero, M.P. Mentruit, C.O. Areán, A. Zecchina, J. Catal. 162 (1996) 268–276.

[38] C.A. Emeis, J. Catal. 141 (1993) 347.),

Table 1

Esterification of levulinic acid with ethanol (reaction conditions: T=70 °C, t=5 h, Et/LA ratio=5:1, 0.05 g of catalyst (2.5 wt.%)).

Catalyst	LA conversion, %	Reusability	Ref.
Amberlyst	54	Stable during 4 cycles	[6]
SO_4^{2-}/ZrO_2	9	*n.r.	[6]
SO_4^{2-}/SnO_2	44	Decrease in conversion to 14 % after second run	[6]
SO_4^{2-}/TiO_2	39	n.r.	[6]
SO_4^{2-}/Nb_2O_5	14	n.r.	[6]
SO_4^{2-}/ZrKIL-2	51	LA conversion of 47 % after 3 reaction cycles	[8]
Nano-SO_4^{2-}/SnO_2	77	Decrease of catalytic activity by 25%, in 3 reaction cycles	[7]
HUSY	8	n.r.	[6]
HBEA	5	n.r.	[6]
HMor	3	n.r.	[6]
HZSM-5	5	n.r.	[6]

*not reported

Table 2

Average chemical compositions of the clinoptilolite phase of the catalysts obtained by EDS analysis.

Sample	Si	Al	O	Na	K	Ca	Mg	Sn	S	Si/Al	S/Sn
	at.%										
CLI	22.9	4.7	69.8	0.2	0.5	1.2	0.7	0.04	–	4.9	–
HCLI	37.8	5.4	69.5	0.04	–	–	–	–	–	7.0	–
TOHCLI5	31.5	4.4	63.2	0.1	–	–	–	0.7	–	7.2	–
STOHCLI5	23.5	3.2	72.6	0.1	–	–	–	0.4	0.3	7.3	0.8
TOHCLI9	21.9	2.8	74.6	–	–	–	–	1.6	–	7.8	–
STOHCLI9	20.2	2.8	75.1	–	–	–	–	1.4	0.5	7.2	0.4
TOHCLI12	20.4	2.7	74.4	0.1	–	–	–	2.4	–	7.6	–
STOHCLI12	18.9	2.5	76.7	–	–	–	–	1.8	0.7	7.6	0.4
RSTOHCLI9	22.3	3.0	72.9	–	–	–	–	1.3	0.3	7.4	0.2

Table 3

Textural properties of samples.

Sample	S_{BET} [a], $m^2\ g^{-1}$	S_{mic} [b], $m^2\ g^{-1}$	S_{ext} [c], $m^2\ g^{-1}$	V_{mic} [d], $cm^3\ g^{-1}$	V_t [e], $m^3\ g^{-1}$	d [f], Å
HCLI	31.6	7.1	24.5	0.0023	0.1204	296
TOHCLI5	39.7	11.1	27.3	0.0048	0.1307	170
STOHCLI5	38.4	9.7	30.0	0.0044	0.0738	224
TOHCLI9	41.6	17.3	24.3	0.0073	0.0760	230
STOHCLI9	33.2	15.5	17.7	0.0095	0.1208	315
TOHCLI12	79.8	14.9	64.9	0.0069	0.0929	150
STOHCLI12	67.9	12.5	52.3	0.0086	0.0880	146

[a] specific surface area based on BET theory determined in the p/p_0 range corresponding to the increasing trend of Rouquerol plot; [b] micropore surface area based on *t*-plot analysis; [c] external surface area $S_{BET} - S_{mic}$; [d] micropore volume based on *t*-plot analysis; [e] total pore volume based on BJH adsorption analysis; [f] average pore size based on BJH desorption analysis.

Table 4

Acidity of the representative samples based on the FTIR spectra of adsorbed pyridine.

Sample	Brønsted sites, μmol g^{-1}	Lewis acid sites, μmol g^{-1}
TOHCLI5	0	55.5
STOHCLI5	117.4	240.0
TOHCLI9	3.8	164.5
STOHCLI9	143.7	236.4

acidity calculated with integrated molar extinction coefficients determined by Emeis et al. [38]: 2.22 cm μmol^{-1} for 1450cm^{-1} band and 1.67 cm μmol^{-1} for 1550 cm^{-1} band.

Figure Captions

Fig. 1. TG (left) and DTG (right) curves of non-sulfated (a, b) and sulfated samples (c, d).

Fig. 2. XPS spectra (left) and Sn concentration profile (right) of STOHCLI5 and STOHCLI9 and XPS depth profile.

Fig. 3. a) ^{27}Al and b) ^{28}Si MAS NMR spectra of selected catalysts.

Fig. 4. Adsorption/desorption isotherms of nitrogen at –196 °C on: a) TOHCLI5, b) STOHCLI5, c) TOHCLI9, d) STOHCLI9, e) TOHCLI12, f) STOHCLI12.

Fig. 5. FTIR spectra of adsorbed pyridine: a) TOHCLI5/STOHCLI5 and b) TOHCLI9/STOHCLI9. Lewis- and Brønsted acid sites are marked by LPy and BPy, respectively. Spectra were collected after Py desorption at 100, 200, 300 and 400 °C, shown from top to bottom for each sample.

Fig. 6. LA conversion in the esterification with octanol (T=100 °C, LA:Oct=1:7).

Fig. 7. LA conversion in the esterification with ethanol (T=100 °C, LA:Et=1:7).

Fig. 8. Reusability of the catalyst STOHCLI9 in LA esterification with a) octanol and b) ethanol at the reaction temperature of 100 °C, LA:Oct/Et ratio=1:7 and reaction time of 5 h in 6 consecutive reaction cycles.

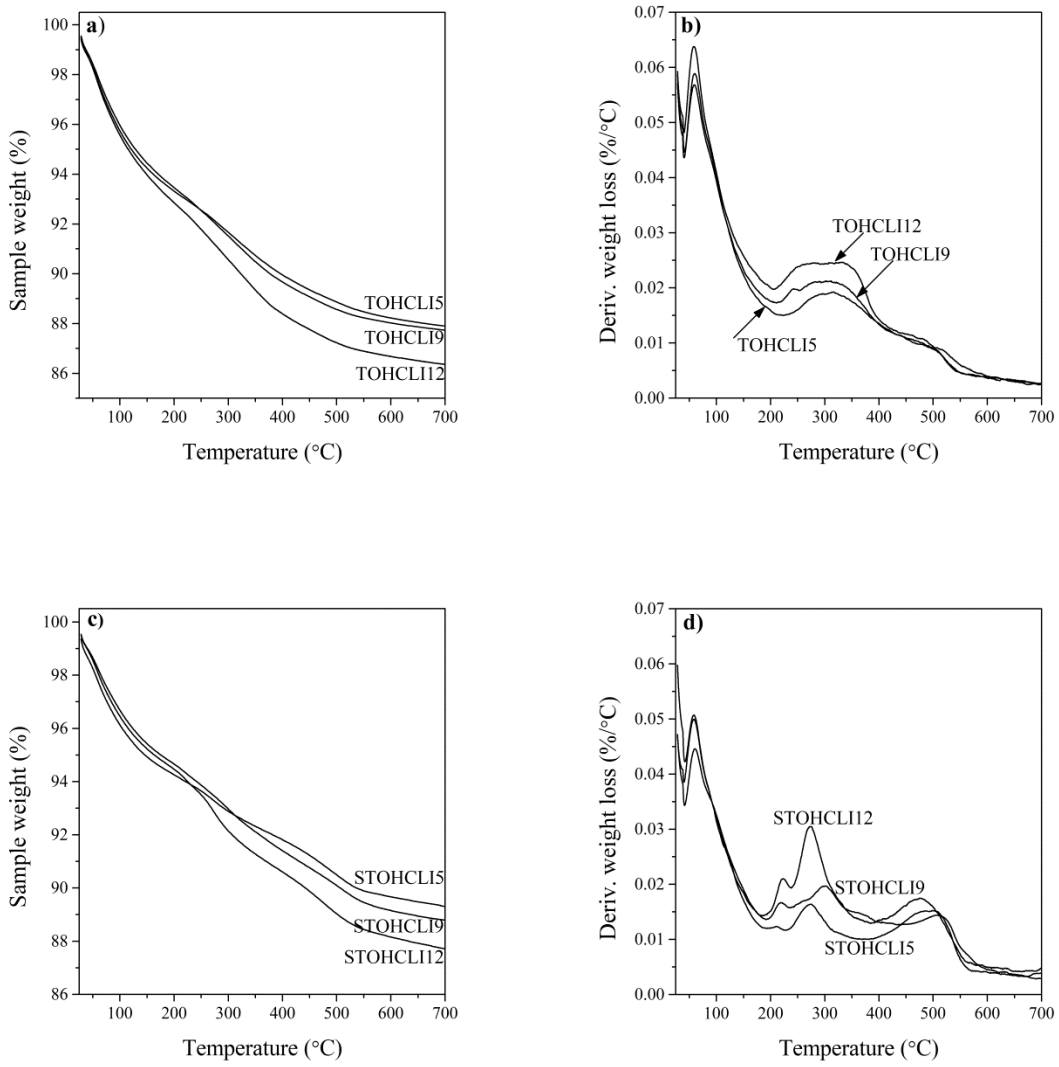

Fig. 1.

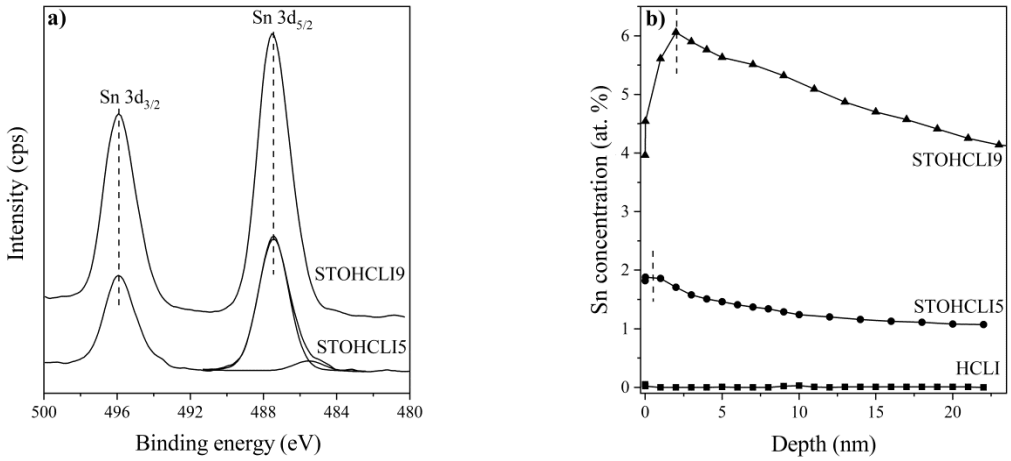

Fig. 2.

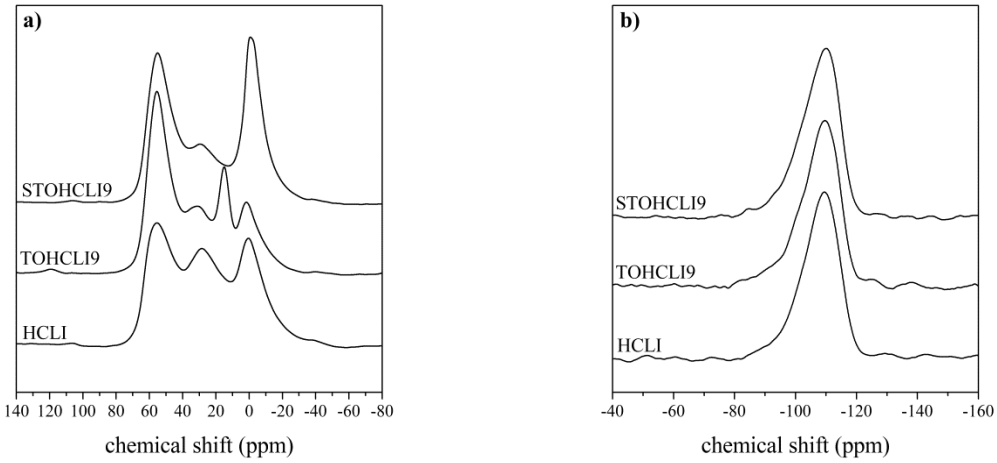

Fig. 3.

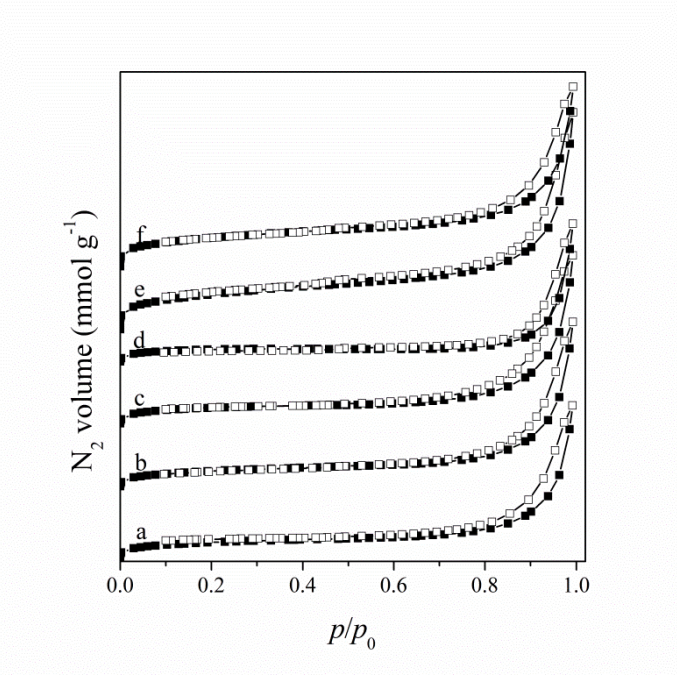

Fig. 4.

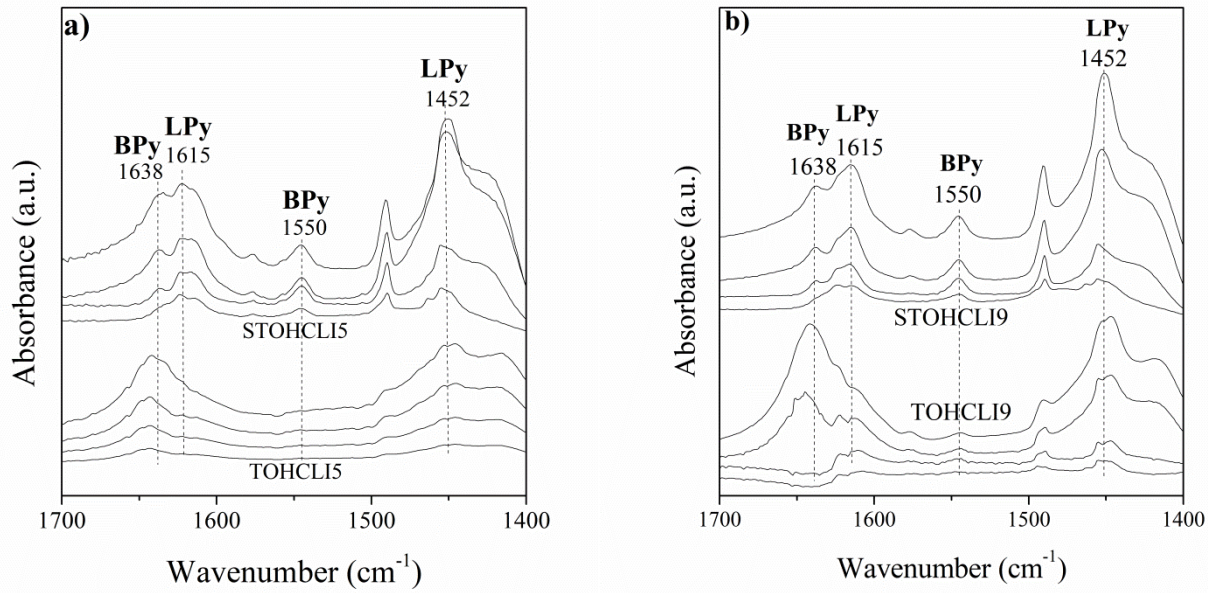

Fig. 5.

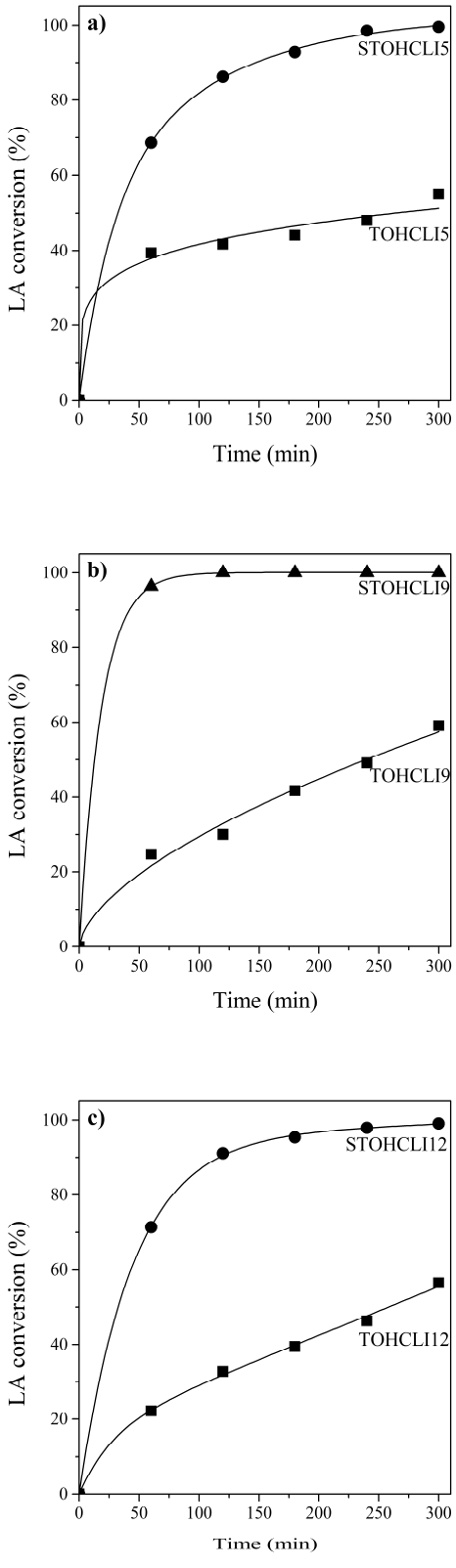
a)
STOHCLI5
TOHCLI5
LA conversion (%)
Time (min)
b)
STOHCLI9
TOHCLI9
LA conversion (%)
Time (min)
c)
STOHCLI12
TOHCLI12
LA conversion (%)
Time (min)

Fig. 6.

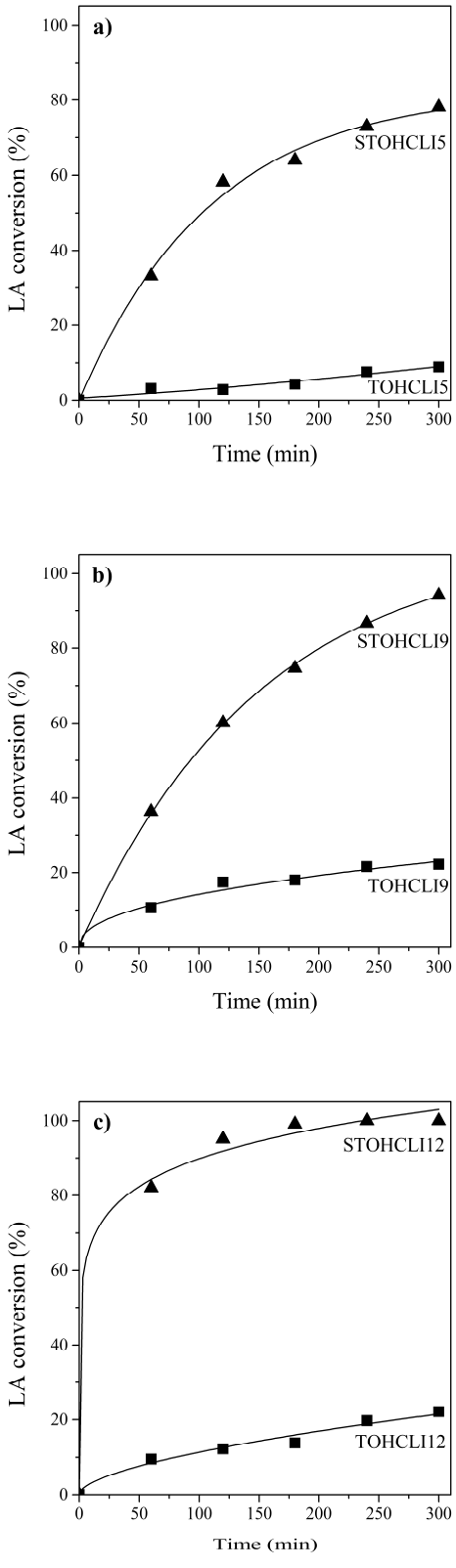
a)
STOHCLI5
TOHCLI5
LA conversion (%)
Time (min)
b)
STOHCLI9
TOHCLI9
LA conversion (%)
Time (min)
c)
STOHCLI12
TOHCLI12
LA conversion (%)
Time (min)

Fig. 7.

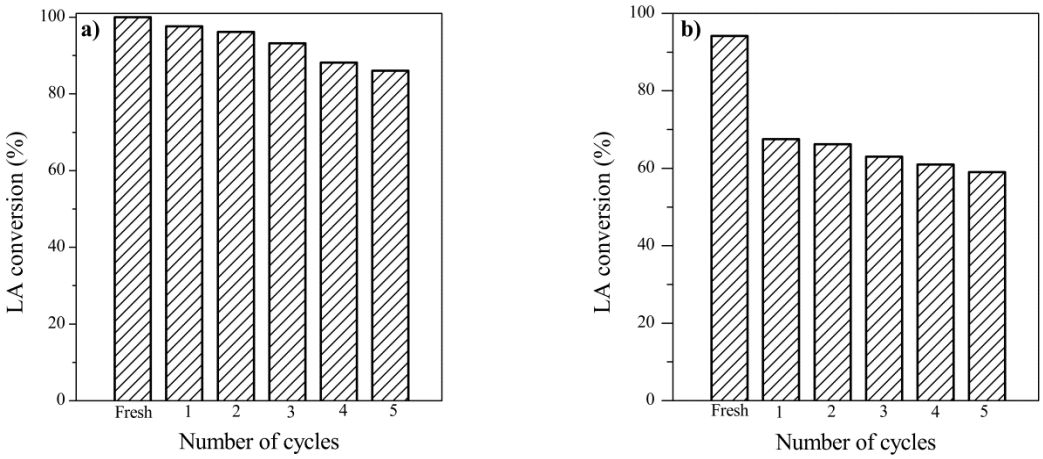

Fig. 8.

Supplemental material

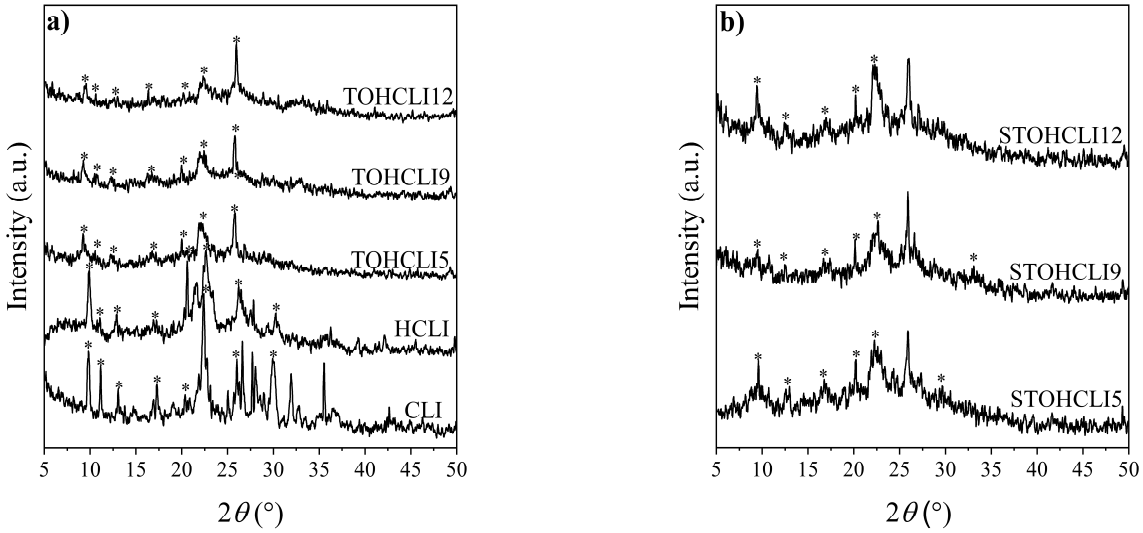

Fig. 1. PXRD pattern of a) CLI, HCLI and non-sulfated and b) sulfated catalysts.

Diffractions from the clinoptilolite phase are marked by asterix (∗).

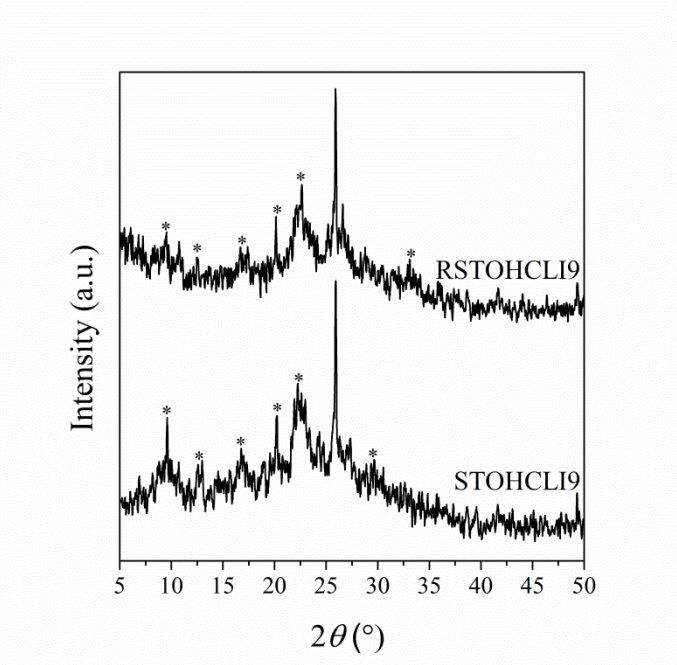

Fig. 2. PXRD pattern of fresh STOHCLI9 and spent (RSTOHCLI9). Diffractions from the clinoptilolite phase are marked by asterix (∗).

- SnO_2-containing clinoptilolite is catalytically active in levulinate production
- Total esterification of renewable levulinic acid to octyl levulinate at 100 ^oC
- Clinoptilolite-based catalysts remain active during 6 esterification cycles